Research Article
doi.org/10.1002/cbic.202400734
Chemistry Europe
European Chemical Societies Publishing

www.chembiochem.org

Cytotoxic Ruthenium(II)-Diphosphine Complexes Affect the Mitochondrial Respiration of Lung Cancer Cells

Marcos V. Palmeira-Mello,*[a, b] Pierre Mesdom,[b] Pierre Burckel,[c] Samia Hidalgo,[c] Olivier Blacque,[d] Gilles Gasser,*[b] and Alzir A. Batista*[a]

In this work, we studied six Ruthenium(II)-diphosphine compounds containing different mercapto ligands (N–S), with general formula $[Ru(N–S)(dppm)_2]Cl$ (dppm = 1,1-*bis*(diphenylphosphino)methane). These compounds were characterized by several techniques (NMR [^1H, $^{31}P\{^1H\}$, and ^{13}C], HRMS, IR, UV-Vis and XRD) and their purity confirmed by elemental analysis. DLS experiments revealed low diameters and polydispersity indexes, and positive log P values in *n*-octanol/PBS indicated their preference for the organic phase. In general, these compounds are stable in different media over 48 h. Cytotoxicity experiments revealed promising IC_{50} values on A549 breast cancer cells, 0.48 μM and 0.80 μM for $[Ru(mtz)(dppm)_2]Cl$ (**1**) and $[Ru(mmi)(dppm)_2]Cl$ (**2**), respectively (mtz and mmi are 2-mercapto-2-thiazoline and mercapto-1-methylimidazole in their deprotonated form, respectively). Clonogenic and migration experiments indicated their antiproliferative and anti-migratory capacity. ICP-MS results indicated their cellular accumulation in the nucleus, with little amounts in mitochondria. No covalent DNA binding was observed by ICP-MS. JC-1 and cell Mito Stress test confirmed mitochondrial dysfunction, which was verified by mitochondrial membrane potential uncoupling and drastic alterations in the oxygen consumption rate. Taken together, our results provide crucial insights regarding the anticancer potential of ruthenium(II)-phosphine compounds.

Introduction

Chemotherapy is the main strategy to fight cancer.[1] The use of metal-based compounds as anticancer agents has been rising with the development of cisplatin and other platinum-based drugs.[2] However, the use of these compounds is limited due to their side effects and resistance.[3] Aiming to overcome this issue, other metals have been intensively studied as potential anticancer agents.[4,5,6] Ruthenium, exhibiting chemical and structural properties different from those presented by the platinum complexes, arises as a promising alternative for this medicinal purpose. Its different oxidation states and ability to form octahedral compounds through different ligands on its coordination sphere are crucial points that make it a focus of medicinal inorganic chemistry.[7,8,9,10] In particular, Ru(II)-phosphine complexes have demonstrated high cytotoxicity against several cancer cell lines and are able to interact with sub-cellular organelles other than nuclei.[11,12,13,14] Mitochondria are found in most of eukaryotic organisms and have been considered as a potential therapeutic target for cancer treatment.[15] These intracellular organelles consist in a double-membrane system, containing inner and outer membranes, and play a crucial role in cellular homeostasis, metabolism and ATP (adenosine triphosphate) production via oxidative phosphorylation (OXPHOS), and its dysfunction is one of hallmarks of the disease.[16,17] Previous reports revealed that ruthenium triarylphosphine complexes exhibit affinity for these organelles, which can lead to mitochondrial dysfunction and cell death via apoptosis. Moreover, it was described that Ru(II) complexes containing both tris(pyrazolyl)methane and triphenylphosphine ligands presented high selectivity toward cancer cells, and act via apoptotic mechanism partly in disrupting mitochondrial calcium balance.[18]

In order to continue our efforts in the development of ruthenium-based anticancer compounds,[19,20,21,22] we report the synthesis and characterization of six Ru(II)-diphosphine compounds containing different mercapto ligands (Figure 1, **1**–**6**). The cytotoxicity of the compounds was investigated in different cell lines. Based on their promising results, compounds **1** and **2** were studied biologically in depth. Migration and clonogenic assays were performed in A549 lung cancer cells. Both compounds are capable of affecting the mitochondrial functions, disrupting the mitochondrial potential and respiration in these cells. Overall, we demonstrate that ruthenium-phosphine-mercapto compounds are efficient cytotoxic anticancer agents.

[a] *M. V. Palmeira-Mello, A. A. Batista*
Departament of Chemistry, Universidade Federal de São Carlos, 13565-905, São Carlos, SP, Brazil
E-mail: marcos.palmeira@ufscar.br
daab@ufscar.br

[b] *M. V. Palmeira-Mello, P. Mesdom, G. Gasser*
Chimie ParisTech, PSL University, CNRS, Institute of Chemistry for Life and Health Sciences, Laboratory for Inorganic Chemical Biology, 75005 Paris, France
E-mail: gilles.gasser@chimeparistech.psl.eu
pierre.mesdom@chimieparistech.psl.eu

[c] *P. Burckel, S. Hidalgo*
Institut de Physique du Globe de Paris, Biogéochimie à l'Anthropocène des Eléments et Contaminants Emergents, 75005 Paris, France

[d] *O. Blacque*
Department of Chemistry, University of Zurich, Winterthurerstrasse 190, 8057 Zurich, Switzerland

Supporting information for this article is available on the WWW under https://doi.org/10.1002/cbic.202400734

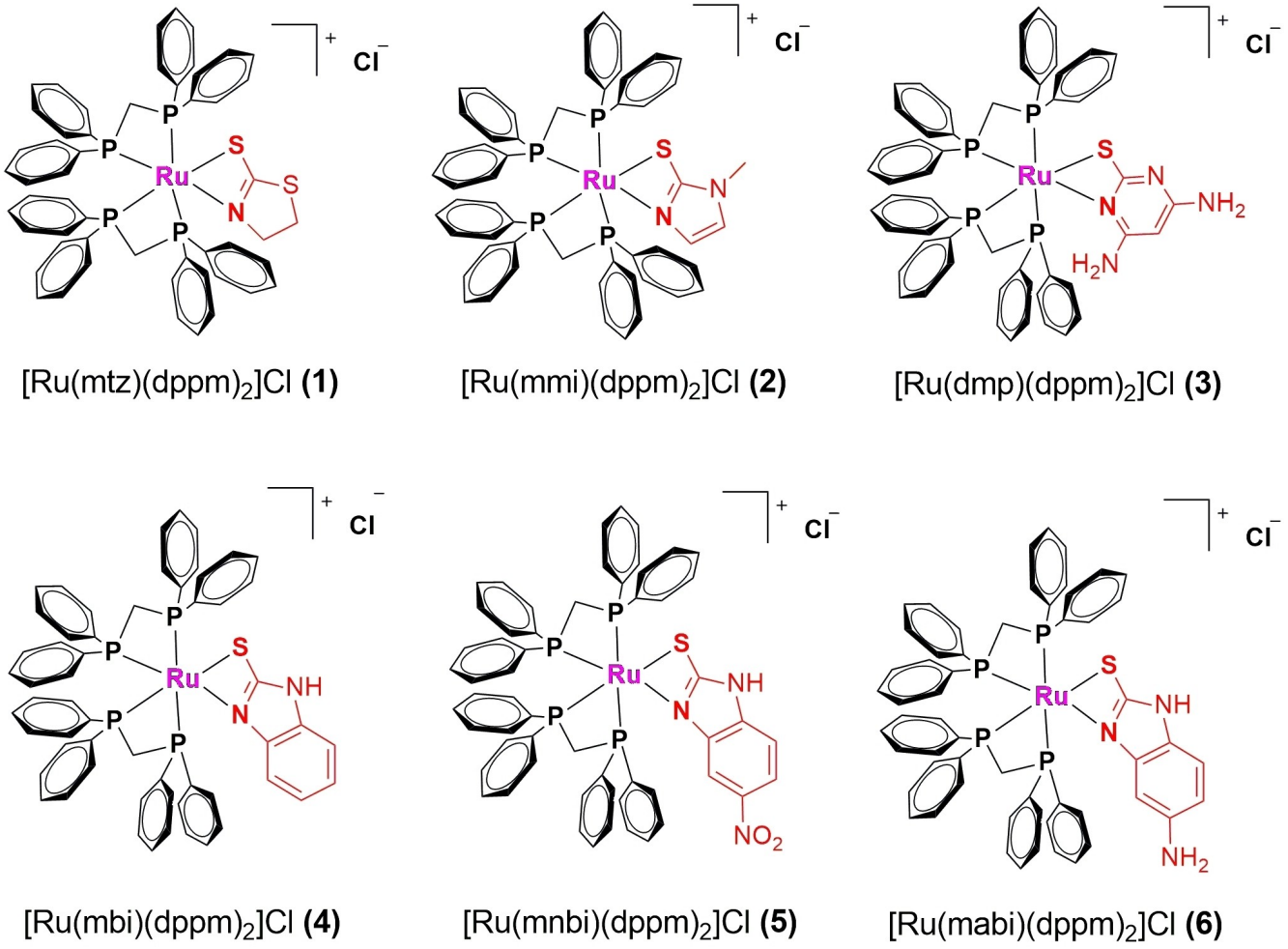

Figure 1. Chemical structures of compounds **1**–**6**.

Results and Discussion

Synthesis and Characterization

The synthesis of the precursor $[RuCl_2(dppm)_2]$ has already been reported (dppm = 1,1-*bis*(diphenylphosphino)methane).[23,24] This compound was characterized by $^{31}P\{^1H\}$ NMR spectroscopy and its purity confirmed by elemental analysis. The compounds **1**–**6** were obtained *via* nucleophilic substitution by refluxing the precursor and the respective mercapto ligand in MeOH in presence of $NaHCO_3$. The final compounds were precipitated with water and isolated by filtration with yield ranging from 45 to 83%. The compounds were characterized by ^1H, $^{31}P\{^1H\}$, ^{13}C NMR and infrared spectroscopies, molar conductivity and high-resolution mass spectrometry (HR-MS). The $^{31}P\{^1H\}$ NMR spectrum of the precursor complex *cis*-$[RuCl_2(dppm)_2]$ shows two triplets at −0.21 and −26.25 ppm, indicating the equivalence of the phosphorus atoms of dppm ligand (J = 36.0 Hz). For compounds **1**–**6**, the $^{31}P\{^1H\}$ NMR shows different data set. For example, compound **1** presents signals at 3.86 (ddd, 1P), −1.07 (ddd, 1P) and −17.28 ppm (ddd, 2P), indicating their non-equivalence. For this compound, ^1H NMR spectrum revealed the aliphatic protons from dppm ligand at 2.0–6.0 ppm, while the aromatic protons from dppm/mercapto ligands can be found in the region between 6.5–8.0 ppm. The IR spectrum revealed the presence of bands related to C=C and C=N bonds of both phosphine and mercapto ligands in the region at 1628–1434 cm^{-1}. The bands around 1098 and 1190 cm^{-1} can be attributed to the P–C and C–S bonds, respectively. A similar behavior was observed for compounds **2**–**6**. The molar conductance obtained in DMSO indicated these compounds as 1:1 electrolytes.[25] Furthermore, their purity was assessed by elemental analysis and LC–MS. Compounds **1**, **2**, **4** and **5** were crystallized by slow evaporation in DCM or DCM:MeOH (1:1), and their structures confirmed by single crystal X-ray diffraction. Crystal data and structure refinement parameters are presented in the supporting information material. In these structures, the Ru(II) ion is coordinated by two dppm ligands and one mercapto, adopting a distorted octahedral geometry with Ru–N bond lengths ranging from 2.16 to 2.18 Å and Ru–S from 2.46 to 2.50 Å, respectively. Compounds **1** and **2** crystalized as a monocationic complex, and a chloride counter-ion was observed in a second coordination sphere. To our surprise, for compounds **4** and **5** we observed a second deprotonation of a

mercaptobenzimidazole ligand, and these compounds crystallized as neutral compounds. In the crystal structure of **1**, the Cl^- counterions are disordered over two positions with site-occupancy factors of 0.712(3) and 0.288(3). Solvent molecules of methanol are also present in the crystal in disordered positions in a ratio 1.71/1 with the main species. In the crystal structure of **2**, the asymmetric unit contains two independent Ru-containing cationic species together with two Cl^- counterions. Solvent molecules of water cocrystallized with the main species in a ratio 1/1/4, respectively. In one of the two cations the mercapto-1-methyl-imidazole (mmi) ligand is disordered over two sets of positions with site-occupancy factors refined to 0.197(2) and 0.803(2). Some SHELXL restraints/constraints had to be used (SADI, SIMU, DFIX) to correct the geometry of the disordered fragments and the anisotropic displacement parameters of the corresponding atoms. In the crystal structure of **4**, the main species cocrystallized with solvent molecules of dichloromethane and water (disordered over different sets of positions). In the crystal structure of **5**, the main species cocrystallized with solvent molecules of water (disordered over different sets of positions). In **4** and **5**, some non-hydrogen atoms (involved in the disorders) were restrained to have similar atomic displacement parameters (Figure 2).

UV-Vis spectra of the compounds were recorded in DMSO and are similar to those already reported for Ru(II)-mercapto complexes.[11] Bands close to 300 nm can be ascribed as metal-to-ligand charge transfer transitions (MLCT). In addition, bands around 350–400 nm can be attributed to MLCT and d–d mixing transitions.

Stability and Physicochemical Properties

Stability is an essential parameter in medicinal chemistry, playing a crucial role on pharmacokinetics/pharmacodynamics (PK/PD) processes. In this scenario, the stability of compounds

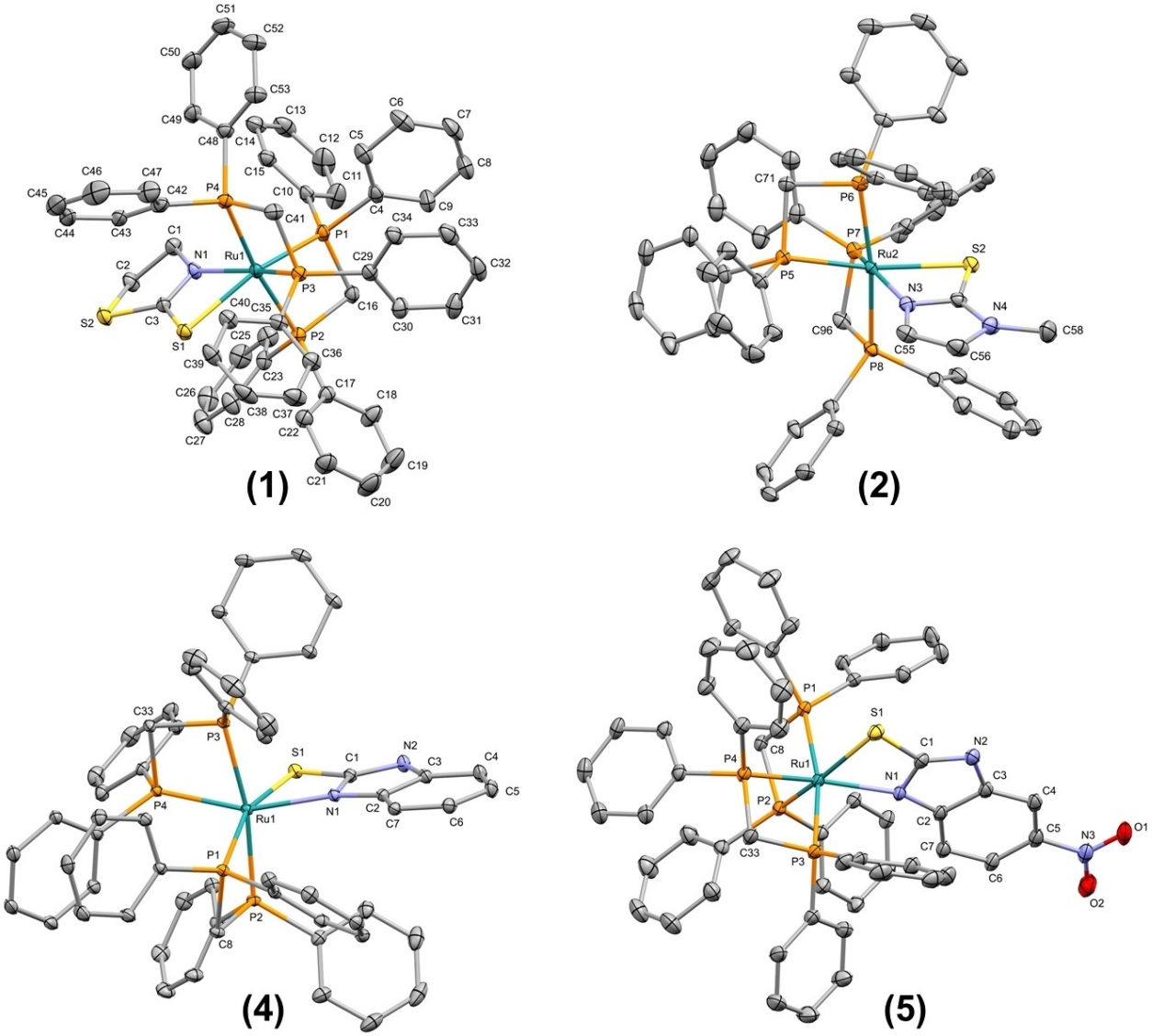

Figure 2. The molecular structure of **1**, **2**, **4** and **5** with displacement ellipsoids drawn at the 30% probability level. Hydrogen atoms and counterions are excluded for clarity.

1–**6** was studied in different media. First, their stability was studied in DMSO and DMSO/PBS solutions by UV-Visible spectroscopy up to 48 h. No significant changes were observed in their spectra, indicating that all compounds are stable in these conditions. Next, solutions of the compounds in DMSO and DMSO/DMEM (80 : 20) were investigated during 48 h by $^{31}P\{^{1}H\}$ NMR. Again, no significant alterations were observed. To obtain a better confidence on their integrity, the stability of all compounds was further evaluated in culture medium by HPLC. Due to their low solubility in biological medium, the compounds were first dissolved in 10–20% DMSO before addition to the DMEM solution. Under these conditions, all compounds presented retention times around 10.73–14.00 min. On the other hand, the retention times for the free ligands can be found in a range between 1.48 and 8.67 min. No significant changes were observed for the complexes after 48 h, confirming their stability. As lipophilicity is an important property related to drug absorption, the distribution coefficient (log P) of the compounds was determined in PBS/octanol. All compounds were mainly found in the organic phase, and compound **5**, which contains a NO_2 group in a benzimidazole moiety, was the most lipophilic compound (log $P = +1.20 \pm 0.19$). As expected, this property is affected by the nature of the groups attached to aromatic ring (log P: **5** > **4** > **6**) (Figure 3A). As some Ru(II)-based compounds can form aggregates in aqueous solutions,[26,27] we used a dynamic light scattering (DLS) analysis to investigate the behavior of our compounds in 10% FBS in PBS. The results revealed the existence of particles with a diameter ranging from 25.30 to 53.45 nm and low polydispersity indexes (PDI) ranging from 0.273 to 0.575 (Figure 3B), which are in agreement with those previously obtained for Ru(II) compounds.[28]

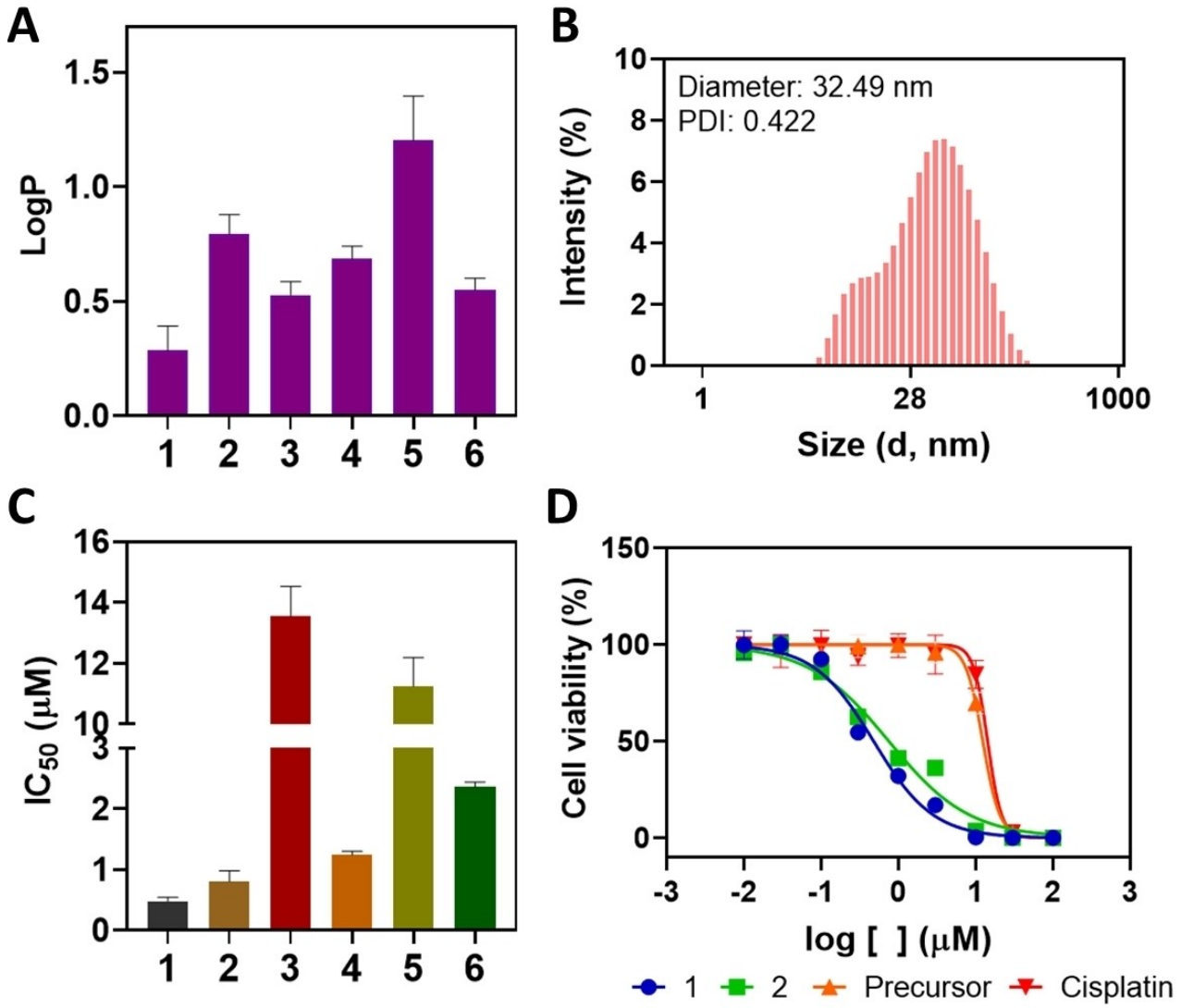

Figure 3. (**A**) Partition coefficient of compounds **1**–**6** between PBS/octanol. (**B**) Size distribution by the intensity of compound **1** (20 μM) in PBS 10% FBS. (**C**) IC_{50} (μM) obtained for compounds **1**–**6** in A549 lung cancer cells. Data are presented as mean ± SD of three independent replicates (**D**) Cell viability (A549) after treatment with compounds **1**, **2**, *cis*-$[RuCl_2(dppm)_2]$ and cisplatin.

In Vitro Cytotoxicity, Clonogenic and Migration Assays

The cytotoxicity of compounds **1**–**6** was investigated in monolayer cultures of mouse colon adenocarcinoma (CT-26), human colon cancer (HT-29), human lung carcinoma (A549) and non-cancerous retinal pigment epithelium (RPE-1) cell lines using alamar blue (resazurin) fluorometric assay. Cisplatin as well as the free mercapto ligands and the precursor *cis*-$[RuCl_2(dppm)_2]$ were tested as controls in the same conditions. The IC_{50} (the half maximal inhibitory concentration) values obtained for these compounds are presented in Table 1.

As presented, all Ru(II) were cytotoxic in all cell lines tested. In general, the compounds had a better performance on A549 lung cancer cells with IC_{50} ranging from 0.48 to 13.55 μM, highlighting $[Ru(mtz)(dppm)_2]Cl$ (**1**) and $[Ru(mmi)(dppm)_2]Cl$ (**2**) (Figure 3C). Moreover, these compounds were 27 and 16 times more active than cisplatin and 26 and 15 times more active than precursor *cis*-$[RuCl_2(dppm)_2]$ ($IC_{50} = 0.48$ and 0.80 μM, respectively) (Figure 3D, Table 1). Regarding the compounds containing the benzimidazole moiety, $[Ru(mbi)(dppm)_2]Cl$ (**4**) presented the best performance. This result revealed that the presence of $-NO_2$ and $-NH_2$ groups attached on the aromatic ring does not increase the cytotoxicity of $[Ru(mnbi)(dppm)_2]Cl$ (**5**) and $[Ru(mabi)(dppm)_2]Cl$ (**6**). Unfortunately, no selectivity was observed for these compounds, since they were also cytotoxic on non-cancerous RPE-1 cells. No correlations between the lipophilicity and cytotoxicity results were observed. Based on their best cytotoxicity results, compounds **1** and **2** have been selected for further biological experiments in A549 cells.

The antiproliferative properties of **1** and **2** in A549 cells were investigated using the clonogenic assay, which measures the ability of a single cell to proliferate by forming a visible colony.[29] As shown in Figure 4, our results revealed a decrease in the number and size of cell colonies after treatment with **1** and **2** in a concentration-dependent manner (Figure 4A). Both compounds act by a similar way, significantly reducing cell survival at concentrations of 0.24 and 0.40 μM, respectively, which are lower than the IC_{50} values (Figure 4B). At concentrations higher than IC_{50}, **1** and **2** cause almost the total disappearance of cell colonies, thus revealing their cytotoxic and cytostatic properties. It should be mention that this effect was already observed for Ru(II)-phosphine-mercapto compounds.[22,26]

Since metastasis are associated to cell migration ability, the effect of **1** and **2** on the migration of A549 cancer cells was investigated using the wound healing assay. For this experiment, $\frac{1}{2}$ IC_{50} was used. A qualitative assessment of cell migration in absence and presence of both compounds during 72 h are presented in Figure 5. In the absence of the compounds, wound closure was complete. In the other hand, compounds **1** and **2** were able to inhibit this closure, suggesting their antimetastatic effect.[30]

Cellular Uptake

The accumulation and distribution of metal-based compounds into the cells are crucial steps for their cytotoxic effect, and can be monitored by several techniques.[31,32] Due their high cytotoxicity, compounds **1** and **2** had their cellular localization investigated by inductively coupled plasma mass spectrometry (ICP-MS). In general, **1** accumulates in A549 cells faster than **2**, with a content of Ru slightly increased for **1**, 17.33 *versus* 13.35 ng per million cells at 1 μM after 45 min incubation. The dose seems to be a pivotal factor for the cellular uptake since the amount of Ru increased almost 6- and 4-fold after treatment with **1** and **2** at 10 μM, respectively (Figure 6, left). The maximum of Ru content is reached at 10 μM after 4 h of incubation, suggesting this time as optimal for the internalization (222.82 and 190.42 ng per million cells for **1** and **2**, respectively), which is in accordance with previous studies for

Table 1. *In vitro* cytotoxicity (IC_{50}, μM) on mouse colon adenocarcinoma (CT-26), human colon cancer (HT-29), human lung carcinoma (A549) and non-cancerous retinal pigment epithelium (RPE-1) cells after 48 h of incubation. Results are presented as a mean ± SD of three independent replicates of IC_{50}.

	CT-26	*HT-29*	*A549*	RPE-1
1	1.41 ± 0.37	0.52 ± 0.01	0.48 ± 0.06	0.44 ± 0.04
2	1.64 ± 0.07	0.99 ± 0.07	0.80 ± 0.18	0.57 ± 0.02
3	14.58 ± 0.66	1.50 ± 0.04	13.55 ± 0.98	3.61 ± 0.16
4	1.62 ± 0.11	2.55 ± 0.22	1.24 ± 0.06	1.11 ± 0.17
5	6.35 ± 0.36	10.59 ± 0.04	11.25 ± 0.94	8.77 ± 0.88
6	4.20 ± 0.25	3.11 ± 0.21	2.36 ± 0.09	4.70 ± 0.10
Hmtz	> 100	> 100	> 100	> 100
Hmmi	> 100	> 100	> 100	> 100
Hdmp	> 100	> 100	> 100	> 100
Hmbi	> 100	> 100	> 100	> 100
Hmnbi	> 100	> 100	> 100	> 100
Hmabi	> 100	> 100	> 100	> 100
cis-$[RuCl_2(dppm)_2]$	7.00 ± 0.28	35.70 ± 1.53	12.71 ± 0.52	15.26 ± 0.39
Cisplatin	5.49 ± 0.38	4.96 ± 0.06	13.27 ± 0.87	13.38 ± 0.84

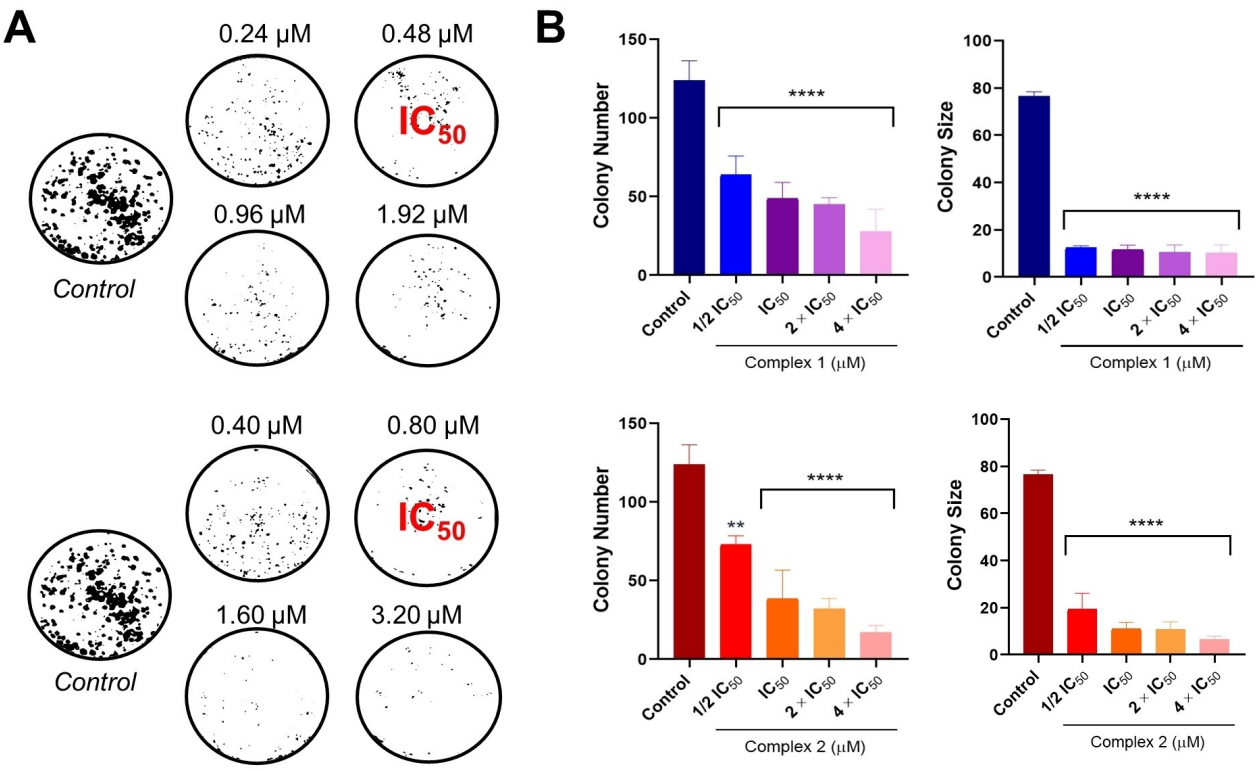

Figure 4. Assessment of the cell survival by clonogenic assay. **(A)** Representative colony formation images of A549 cells after treatment with different concentrations of **1** (top) and **2** (bottom). The study was performed in triplicate and the image represents one of them. **(B)** Quantitative data representing the colony number and size with relation to the concentration of **1** and **2**. (n = 3, one way ANOVA test followed by Dunnett's test). Data are expressed as means ± SD (** $P < 0.01$ and **** $P < 0.0001$).

Ru(II) complexes.[26] To assess the subcellular distribution of these compounds in A549 cells, cell fractionation was performed following treatment with the Ru compounds at 1 and 10 μM. The percentages of metal in the nucleus and mitochondria from A549 cells are presented in Figure 6 (right). At lower concentrations, **1** and **2** present a dynamics of internalization, mainly accumulating in the nucleus (8–15%) with a limited amount in the mitochondria (1–2%). At higher concentrations, the content for **2** in the nucleus is increased twofold (31%), possibly due to its higher lipophilicity, which enabled the entry of **2** through the membrane and reaching the nucleus.

DNA Metallation

Nuclear DNA has been assumed to be the main target for metal-based compounds since the discovery of the mode of action of cisplatin. Therefore, as **1** and **2** were mainly found in the nucleus, their covalent interaction with DNA was investigated.[32] A549 cells were treated with compounds **1** and **2** (10 μM) for 4 h, and the nucleus was isolated from the cells. The DNA-bound Ru was measured by ICP-MS and the results are presented in Figure S69 (Supporting information). To our surprise, no difference in Ruthenium amount between control-DNA and Ru-compounds-DNA was observed, indicating that **1** and **2** are not covalently binding to DNA.

Mitochondrial Functions and Cell Respiration

It is reported that phosphine-based metal complexes are able to cause mitochondrial dysfunction.[12,33] Since our results revealed that DNA was not the main target for **1** and **2**, we decided to focus on mitochondria. First, we investigated the effect of **1** and **2** on the mitochondrial membrane potential (MMP, $\Delta\psi_m$) on A549 cells. MMP is an important parameter commonly studied to evaluate mitochondrial damage. For this experiment, JC-1 fluorescent probe was used. JC-1 is a cationic $\Delta\psi_m$ indicator that can exist in two different forms. When accumulated in healthy mitochondria, JC-1 presents an aggregated form, emitting fluorescence at 590 nm (red). In the other hand, in depolarized mitochondria, JC-1 becomes a monomeric form, and emits fluorescence at 529 nm (green). As shown in Figure 7, in the absence of Ru(II) compounds, a red fluorescence is observed. However, the green fluorescence arises after treatment with **1** and **2**, revealing JC-1 in its monomeric form (Figure 7A). This finding is in agreement with JC-1 fluorescence ratio (red/green) obtained after treatment with **1** and **2** at different concentrations (Figure 7B). At this point, our results indicate that both compounds cause a $\Delta\psi_m$ decreasing, implying in a mitochondrial loss of function, which is an event commonly associated to apoptosis-induced cell death.[34,35]

In a second part of our study, we investigated the mitochondrial respiratory chain, which is essential for the generation and conversion of energy. This chain is composed

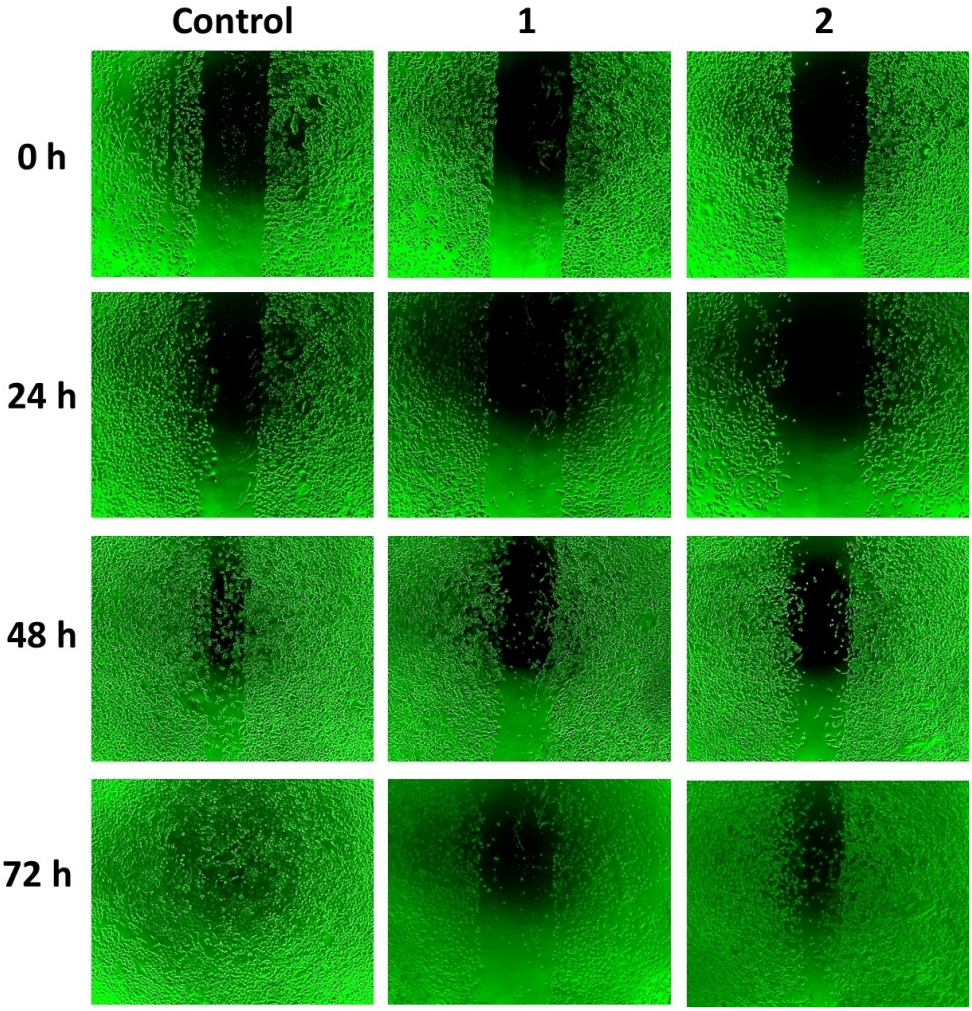

Figure 5. Qualitative assessment of cell migration of A549 cells in an absence and presence of **1** and **2**. DMSO was employed as a negative control.

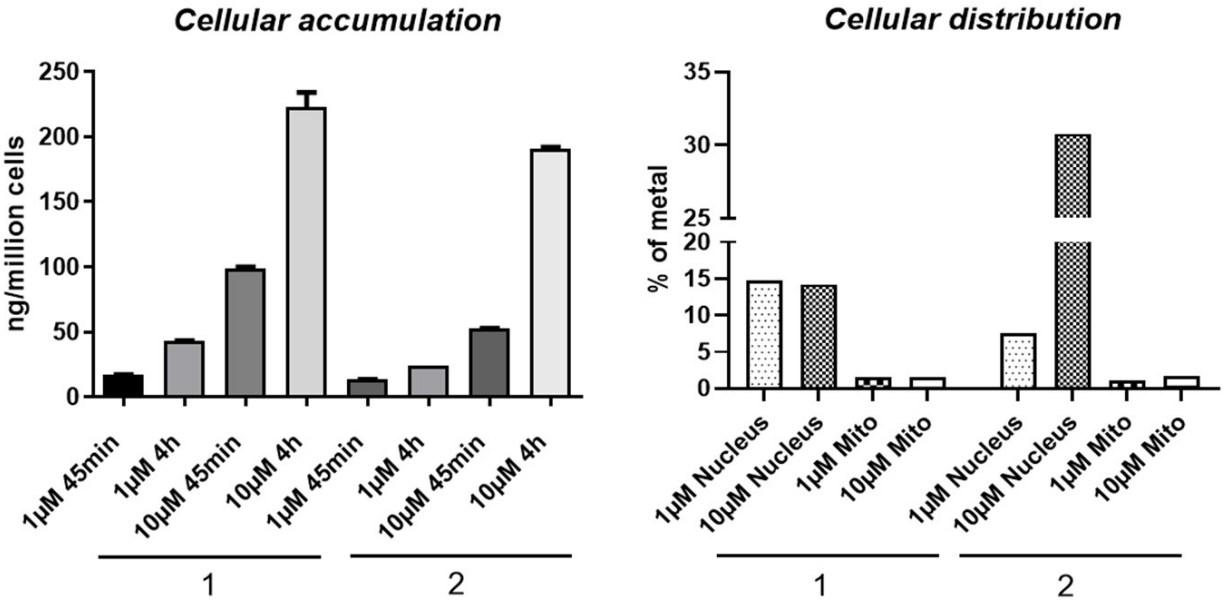

Figure 6. Cellular uptake of compounds **1** and **2**. cellular accumulation (left) and distribution (right) in A549 cancer cells (1 and 10 μM). Data are presented as mean ± SD of two independent replicates.

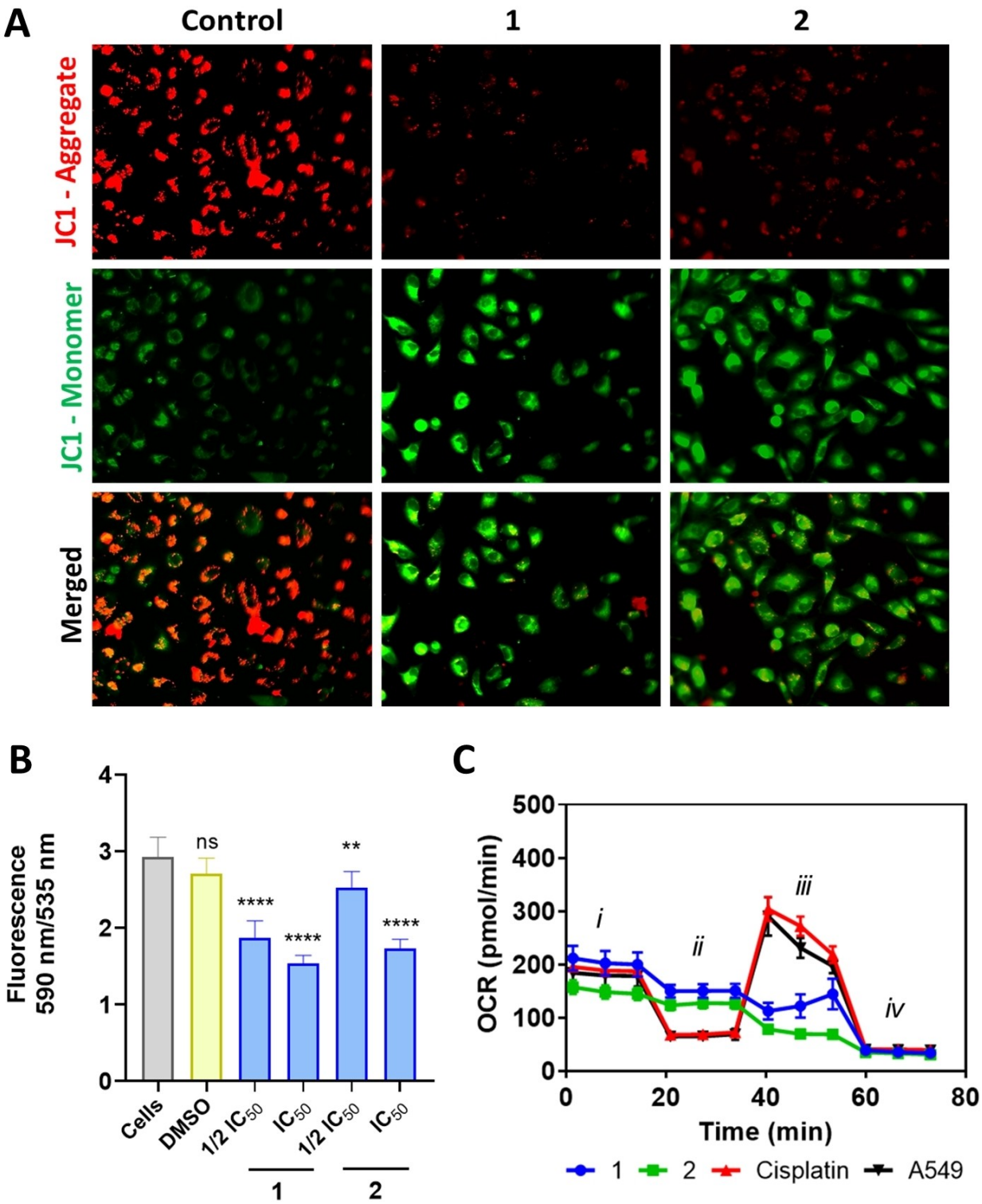

Figure 7. (A) Fluorescence images and (B) signal of the JC-1 dye detected in A549 cancer cells treated for 24 h with **1** and **2**. (n = 7, one way ANOVA test followed by Dunnett's test) (C) Mito stress test profile after 4 h of treatment with **1** and **2**; the oxygen consumption rate (OCR) changes after treatment with specific electron-transport chain inhibitors. Oligomycin (inhibitor of ATP synthase (complex V)), FCCP (uncoupling agent), antimycin-A (complex III inhibitor), and rotenone (complex I inhibitor). For (**B**), data are expressed as means ± SD (** $P < 0.01$, and **** $P < 0.0001$).

by four subunits labeled complex I (NADH : ubiquinone oxidoreductase), complex II (succinate dehydrogenase), complex III (cytochrome bc1 complex), and complex IV (cytochrome c oxidase). Complexes I, III, and IV are proton pumps and provide the gradient across the IMM which energy is used to produce ATP by complex V (ATP synthase). As this process, known as oxidative phosphorylation (OXPHOS), is dependent of cellular oxygen consumption, we decided to evaluate the impact of

compounds **1** and **2** on mitochondrial respiration in A549 cells using a Seahorse XF instrument. To achieve this, a Mito Stress Test was performed[36] after 4 hours of treatment with the IC_{25} concentration of the ruthenium compounds as compared to two controls: cisplatin (IC_{25}) and non-treated cells. The oxygen consumption rate (OCR) was obtained after sequential injections of oligomycin (ATP synthesis inhibitor), carbonyl cyanide-4 (trifluoromethoxy)phenylhydrazone (FCCP) (uncoupling agent), antimycin-A and rotenone (complex III and I inhibitor, respectively), The results presented in Figure 7C and Figure 8 revealed different OCR from cells in the absence and presence of Ru(II) compounds. In general, both compounds **1** and **2** affect the OXPHOS process as compared to controls which present a normal respiration profile.[37,38] Furthermore, the basal OCR only suggests a slight toxicity of **2** (Figure 7C, *i*), indicating that **1** does not affect basal respiration (Figure 8, 'Basal respiration'). However, the treatment with oligomycin does not affect the OCR of the cells treated with the compounds whereas control cells show strongly reduced OCR (Figure 7C, *ii*). Also, the treatment with FCCP, supposed to increase the OCR up to the maximum rate of the cell because of its uncoupling effect (as seen in controls), does not affect OCR of the cells treated with the compounds (Figure 7C, *iii*). Finally, after treatment with rotenone and antimycin, all OCR dropped at the same level, below basal respiration (Figure 7C, *iv*). These results suggest that our compounds act as uncoupling agents (Figure 8, 'Coupling Efficiency'), affecting the mitochondria membrane. This is illustrated by the lack of response after oligomycin treatment (Figure 7C, *ii*) and the low ATP production (Figure 8 'ATP production'). Similar effects have been reported for other metal-based compounds.[39] Also, several parameters of mitochondrial functions were studied as reported.[40,41]

OCR study has shown that the levels of ATP are drastically affected on A549 cells upon incubation with $[Ru(mtz)(dppm)_2]Cl$ (**1**) and $[Ru(mmi)(dppm)_2]Cl$ (**2**) which is in accordance with the potential uncoupling effect of these compounds. Moreover, the spare respiration capacity (difference between maximal respiration and basal respiration) is reduced upon treatment with both compounds, indicating that A549 cells are unable to respond to an energetic demand (Figure 8). Taken together, our results suggest mitochondrial dysfunction as one of the consequences of the modes of action for **1** and **2**.

Conclusions

In this work, we report the synthesis and the biological investigation of new ruthenium(II)-diphosphine-mercapto compounds as potential anticancer agents. The compounds were found to cytotoxic on several cell lines, highlighting $[Ru(mtz)(dppm)_2]Cl$ (**1**) and $[Ru(mmi)(dppm)_2]Cl$ (**2**) on A549 lung cancer cells. Clonogenic and wound healing assays revealed their antiproliferative and antimetastatic properties. Both compounds are able to affect the mitochondrial membrane

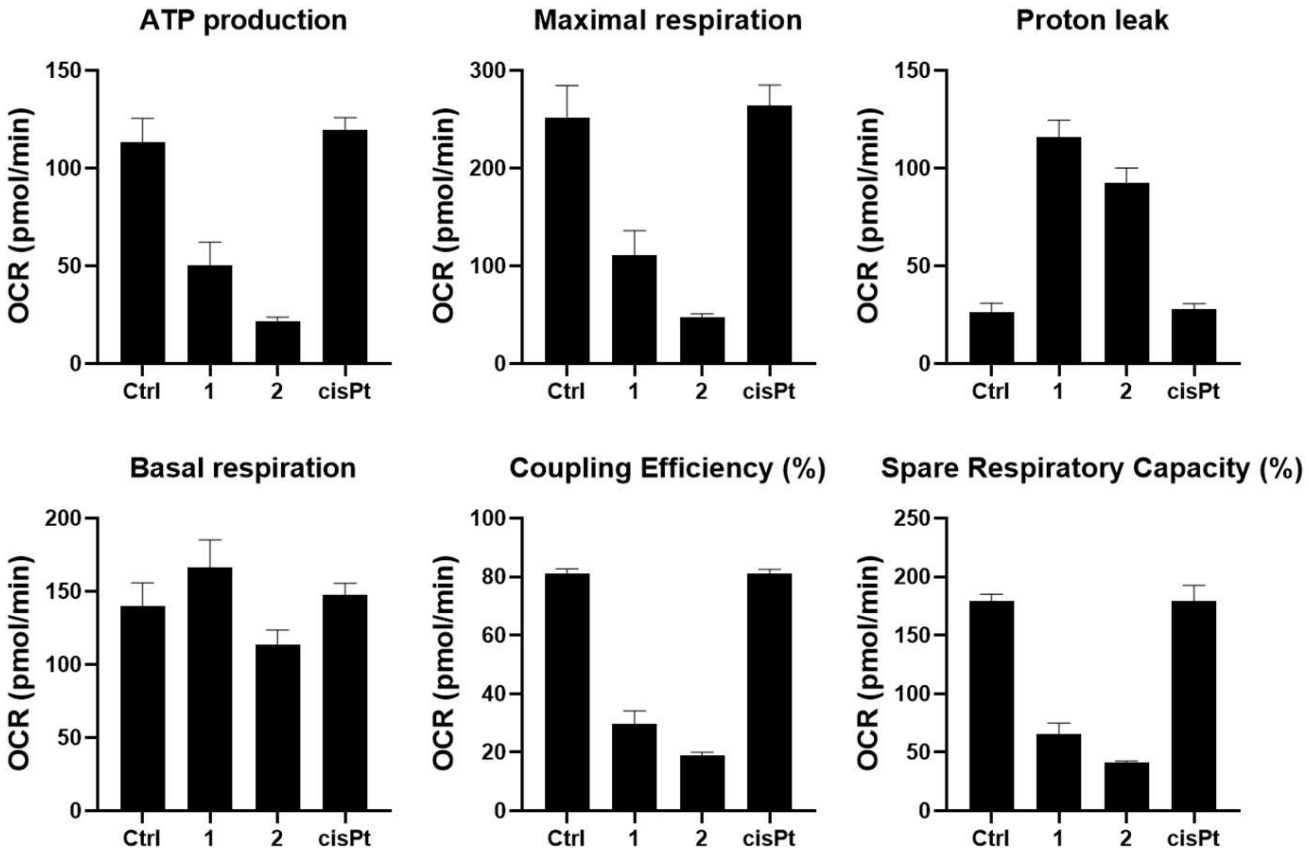

Figure 8. Key parameters of mitochondrial respiration after treatment with different compounds for 4 h.

potential and alter the oxygen consumption rate, confirming mitochondrial dysfunction. Taken together, our findings provide valuable insights into the cytotoxic potential of Ruthenium-based compounds containing mercapto and phosphine moieties.

Experimental Section

Materials and Instrumentation. All chemicals were used as purchased from commercial sources without additional purification. $RuCl_3 \cdot 3H_2O$, 1,1′-*bis*(diphenylphosphine)methane (dppm), 2-mercapto-2-thiazoline (Hmtz), mercapto-1-methylimidazole (Hmmi), 4,6-diamino-2-mercapto-pyrimidine (Hdmp), 2-mercaptobenzimidazole (Hmbi), 2-mercapto-5-nitrobenzimidazole (Hmnbi) and 2-mercapto-5-aminobenzimidazole (Hmabi) ligands were provided by Sigma Aldrich. All solvents were of analytical or HPLC grade. When necessary, solvents were degassed by purging with dry, oxygen-free nitrogen for at least 30 min before use. ^{1}H, ^{31}P, ^{13}C and HSQC NMR spectra were recorded on a Bruker DRX 400 MHz, Bruker Avance III HD 400 MHz or Bruker Avance Neo 500 MHz spectrometers using CH_2Cl_2/D_2O or DMSO-d_6, and using the signal of the deuterated solvent as an internal standard. The chemical shifts (δ) are reported in ppm (parts per million) relative to tetramethylsilane (TMS) or signals from the residual protons of deuterated solvents. Coupling constants *J* are given in Hertz (Hz). Conductivity values were obtained, at room temperature, using 1.0 mM solutions of the complexes in DCM in a Meter Lab CDM2300 instrument. ESI-HRMS experiments were carried out using a LTQ-Orbitrap XL from Thermo Scientific (Thermo Fisher Scientific, Courtaboeuf, France) and operated in positive ionization mode, with a spray voltage at 3.6 kV. Sheath and auxiliary gas were set at a flow rate of 5 and 0 arbitrary units (a.u.), respectively. The voltages applied were 40 and 100 V for the ion transfer capillary and the tube lens, respectively. The ion transfer capillary was held at 275 °C. Detection was achieved in the Orbitrap with a resolution set to 100.000 (at m/z 400) and a m/z range between 200–2000 in profile mode. Spectrum was analysed using the acquisition software XCalibur 2.1 (Thermo Fisher Scientific, Courtaboeuf, France). The automatic gain control (AGC) allowed accumulation of up to 2×10^5 ions for FTMS scans, Maximum injection time was set to 300 ms and 1 μscan was acquired. Infrared spectra were recorded in a SpectrumTwo FTIR Spectrometer (Perkin–Elmer) equipped with a Specac Golden GateTM ATR (attenuated total reflection) accessory; applied as neat samples; $1/\lambda$ in cm^{-1}. Elemental analyses were performed in the Microanalytical Laboratory at the Universidade Federal de São Carlos, São Carlos, Brazil, with an EA 1108 microanalyzer (Fisons Instruments) or at the faculty of pharmacy of Chatenay Malabry, Paris-Saclay University using a Thermo Fisher (Carlo Erba) Flash 2000 Elemental Analyzer. Analytical HPLC measurement was performed using the following system: 2× Agilent G1361 1260 Prep Pump system with an Agilent G7115 A 1260 DAD WR Detector equipped with an Agilent Pursuit XRs 5 C18 (100 Å, C18 5 μm 250×4.6 mm) Column and an Agilent G1364B 1260-FC fraction collector. The solvents (HPLC grade) were acetonitrile (0.1% TFA, solvent A) and millipore water (0.1% TFA, solvent B). The HPLC gradients used are as follows: 0–3 min: isocratic 95% B (5% A); 3–17 min: linear gradient from 95% B (5% A) to 0% B 100% A); 17–23 min: isocratic 0% B (100% A); 23–25 min: linear gradient from 0% B (100% A) to 95% B (5% A). The flow rate was 1 mL/min. Detection was performed at 250 nm with a slit of 4 nm. The UV–Vis spectra were recorded on a Hewlett-Packard 8452 A diode array or in a Varian Cary 8454″ spectrophotometer using a 1 cm path length quartz cuvette. Conductivity values were obtained, at room temperature, using 1.0 mM solutions of the complexes in DMSO in a Meter Lab CDM2300 instrument.

X-ray crystallography. Single crystal X-ray diffraction data were collected at 160.0(1) K on a Rigaku OD Synergy/Hypix diffractometer (**1**, **2** and **5**) or on a Rigaku OD Supernova/Atlas diffractometer (**4**) using the copper X-ray radiation ($\lambda = 1.54184$ Å) from a dual wavelength X-ray source and an Oxford Instruments Cryojet XL cooler. The selected suitable single crystals were covered with oil (Infineum V8512, formerly known as Paratone N), mounted on a flexible nylon loop attached to a CrystalCap Magnetic™ pin (Hampton Research) and transferred to the goniometer head inside the diffractometer.

Pre-experiment, data collection, data reduction and analytical absorption correction[42] were performed with the program suite *CrysAlisPro*.[43] Using *Olex2*,[44] the structures were solved with the SHELXT[45] small molecule structure solution program and refined with the *SHELXL2018/3* program package[46] by full-matrix least-squares minimization on F^2. *PLATON*[47] was used to check the result of the X-ray analysis. Deposition Numbers 2369187 (for **2**), 2369188 (for **1**), 2369189 (for **4**) and 2369190 (for **5**) contain the supplementary crystallographic data for this paper. These data are provided free of charge by the joint Cambridge Crystallographic Data Centre and Fachinformationszentrum Karlsruhe Access Structures service.

Synthesis of compounds. The complexes were obtained from the *cis*-[$RuCl_2(dppm)_2$] precursor. To a solution of a mercapto ligand (0.12 mmol, Hmtz: 24 mg, Hmmi: 23 mg, Hdmp: 28 mg, Hmbi: 30 mg, Hmnbi: 39 mg, Hmabi: 33 mg) and $NaHCO_3$ (18 mg, 0.21 mmol) in methanol previously degassed, *cis*-[$RuCl_2(dppm)_2$] (150 mg, 0.16 mmol) was added. The system was kept under stirring and reflux for approximately 12 h. The volume of the solution was reduced and the powder was filtered off, washed with water and ethyl ether, and dried under reduced pressure.

Precursor *cis*-[$RuCl_2(dppm)_2$]: ^{31}P NMR (162 MHz, D_2O, 298 K) δ/ppm = −0.21 (t, J = 36.0 Hz), −26.25 (t, J = 36.0 Hz). Elemental analysis Calcd for $C_{50}H_{44}Cl_2P_4Ru + 0.5CH_3OH$ (%): C, 63.39; H, 4.35; Found: C, 63.43; H, 4.54. IR: ν(cm^{-1}): 3141.66, 3053.65, 3002.21, 2921.03, 1968.33, 1876.82, 1806.51, 1774.59, 1667.45, 1601.65, 1585.70, 1571.55, 1483.41, 1386.91, 1434.34, 1305.97, 1344.57, 1277.91, 1193.25, 1157.18, 1098.57, 1027.97, 999.34, 964.11, 913.19, 862.69, 844.07, 732.93, 696.51, 722.25, 665.42, 616.01.

[Ru(mtz)(dppm)$_2$]Cl (**1**): 127 mg, 0.124 mmol, 77%. ^{1}H NMR (400 MHz, DMSO-d_6, 298 K) δ/ppm = 7.92–7.81 (m, 4H), 7.69 (t, J = 7.3 Hz, 2H), 7.65–7.58 (m, 3H), 7.56–7.20 (m, 22H), 7.12–7.04 (m, 2H), 6.98 (td, J = 8.9, 1.6 Hz, 4H), 6.49 (ddd, J = 47.0, 11.0, 8.0 Hz, 4H), 5.90–5.77 (m, 1H), 5.45–5.31 (m, 1H), 4.50–4.20 (m, 2H), 3.58 (dt, J = 13.5, 8.9 Hz, 1H), 3.23 (td, J = 9.3, 5.9 Hz, 1H), 2.38 (dd, J = 18.5, 9.3 Hz, 1H), 2.29–2.20 (m, 1H).^{13}C NMR (101 MHz, DMSO-d_6, 298 K) δ/ppm = 182.22, 137.29, 136.15, 134.91, 134.66, 134.48, 134.30, 133.68, 133.33, 133.15, 133.01, 132.77, 131.70, 131.57, 131.46, 131.37, 131.13, 130.94, 130.81, 130.26, 130.07, 130.01, 129.80, 129.70, 129.42, 129.23, 129.12, 128.79, 128.71, 128.61, 128.52, 128.15, 128.05, 59.28, 41.07, 30.86. ^{31}P NMR (162 MHz, DMSO-d_6, 298 K) δ/ppm = 3.86 (ddd, J = 35.1, 32.7, 24.6 Hz), −1.07 (ddd, J = 37.9, 32.2, 24.3 Hz), −17.28 (ddd, J = 36.0, 31.8, 19.4 Hz). HRMS (ESI) m/z: [M]+ Calcd for $C_{53}H_{48}NP_4RuS_2$ 988.1217; Found 988.1233. Elemental analysis Calcd for $C_{53}H_{48}ClNP_4RuS_2$ (%): C, 62.20; H, 4.73; N, 1.37; Found: C, 62.41; H, 4.87; N, 1.58. UV-Vis (DMSO): λ_{max} (ε×10^3 $M^{-1}cm^{-1}$): 354 nm (3.65). IR: ν(cm^{-1}): 3657.67, 3286.40, 3165.97, 3048.77, 2982.94, 2895.47, 2848.27, 2054.69, 1899.85, 1971.00, 1815.47, 1628.84, 1584.76, 1571.59, 1483.91, 1517.28, 1434.34, 1309.38, 1189.55, 1158.79, 1098.12, 1047.29, 997.60, 945.03, 848.89, 728.19, 697.42, 672.46. Molar conductance (μS cm^{-1},

DMSO): 61.8. Analytical HPLC: acetonitrile (solvent A) and milliQ water (solvent B). T_R = 13.838 min.

[Ru(mmi)(dppm)$_2$]Cl (**2**): 135 mg, 0.132 mmol, 82%. ^{1}H NMR (400 MHz, DMSO-d_6, 298 K) δ/ppm = 7.91–7.84 (m, 2H), 7.67–7.59 (m, 2H), 7.56–7.10 (m, 25H), 6.98 (dt, *J* = 13.4, 6.0 Hz, 4H), 6.76 (s, 1H), 6.75–6.60 (m, 4H), 6.56–6.47 (m, 2H), 5.70 (s, 1H), 5.66–5.53 (m, 1H), 5.41–5.30 (m, 1H), 4.71 (dd, *J* = 27.0, 10.2 Hz, 1H), 4.32 (dd, *J* = 27.1, 10.6 Hz, 1H), 3.16 (s, 3H). ^{13}C NMR (101 MHz, DMSO-d_6, 298 K) δ/ppm = 154.80, 138.13, 137.20, 136.89, 135.63, 135.26, 133.52, 133.16, 132.48, 132.11, 132.01, 131.68, 131.58, 131.19, 131.09, 130.83, 130.73, 130.42, 130.29, 130.17, 129.91, 129.81, 129.51, 129.16, 129.07, 128.97, 128.87, 128.73, 128.63, 128.40, 128.14, 128.04, 125.14, 124.43, 118.51, 56.03, 43.28, 43.04, 41.98, 41.73, 41.49, 33.39, 30.26. ^{31}P NMR (162 MHz, DMSO-d_6, 298 K) δ/ppm = 3.86 (ddd, *J* = 35.1, 32.7, 24.6 Hz), −1.07 (ddd, *J* = 37.9, 32.2, 24.3 Hz), −17.28 (ddd, *J* = 36.0, 31.8, 19.4 Hz). HRMS (ESI) m/z: [M]+ Calcd for $C_{54}H_{49}N_2P_4RuS$ 983.1605; Found 983.1623. Elemental analysis Calcd for $C_{54}H_{49}ClN_2P_4RuS + H_2O$ (%): C, 62.58; H, 4.96; N, 2.70; Found: C, 62.74; H, 5.06; N, 2.94. UV-Vis (DMSO): λ_{max} (ε×10^3 M^{-1} cm^{-1}): 348 nm (2.64), 406 nm (0.78). IR: ν(cm^{-1}): 3658.11, 3305.01, 3052.06, 2983.65, 1966.65, 1584.83, 1628.33, 1518.85, 1572.01, 1466.47, 1434.75, 1484.12, 1392.66, 1319.13, 1282.37, 1189.44, 1147.75, 1098.22, 1025.77, 998.97, 927.30, 850.54, 730.39, 700.14, 616.64. Molar conductance (μS cm^{-1}, DMSO): 61.4. Analytical HPLC: acetonitrile (solvent A) and milliQ water (solvent B). T_R = 13.731 min.

[Ru(dmp)(dppm)$_2$]Cl (**3**): 140 mg, 0.133 mmol, 83%. ^{1}H NMR (400 MHz, DMSO-d_6, 298 K) δ/ppm = 8.02 (s, 4H), 7.66 (s, 3H), 7.56 (s, 5H), 7.43–7.03 (m, 22H), 6.94 (d, *J* = 20.8 Hz, 4H), 6.84–6.51 (m, 4H), 6.23 (s, 2H), 5.69 (s, 1H), 5.56 (s, 1H), 5.00 (s, 1H), 4.86 (dd, *J* = 25.4, 10.3 Hz, 1H), 4.38 (dd, *J* = 25.4, 10.3 Hz, 1H). ^{13}C NMR (101 MHz, DMSO-d_6, 298 K) δ/ppm = 181.25, 162.86, 162.71, 138.97, 138.70, 138.40, 138.14, 137.50, 137.37, 137.20, 137.04, 135.42, 135.32, 135.08, 134.98, 134.77, 134.31, 134.24, 134.00, 133.94, 132.06, 131.96, 131.70, 131.60, 131.32, 131.22, 131.14, 131.04, 130.50, 130.39, 129.87, 129.60, 129.33, 129.23, 129.13, 128.70, 128.61, 128.53, 128.43, 128.35, 128.26, 127.87, 127.77, 78.82, 41.77, 41.53, 41.19, 40.95. ^{31}P NMR (162 MHz, DMSO-d_6, 298 K) δ/ppm = 0.20 (ddd, *J* = 40.7, 27.9, 23.8 Hz), −12.61 (dt, *J* = 33.8, 24.0 Hz), −14.42 (ddd, *J* = 327.8, 40.7, 24.5 Hz), −25.74 (ddd, *J* = 327.8, 33.8, 29.1 Hz). HRMS (ESI) m/z: [M]+ Calcd for $C_{54}H_{49}N_4P_4RuS$ 1011.1666; Found 1011.1673. Elemental analysis Calcd for $C_{54}H_{49}ClN_4P_4RuS + 0.5H_2O$ (%): C, 61.45; H, 4.78; N, 5.31; Found: C, 61.45; H, 4.36; N, 5.44. UV-Vis (DMSO): λ_{max} (ε×10^3 M^{-1} cm^{-1}): 306 nm (8.85), 353 nm (2.65), 406 nm (1.11). IR: ν(cm^{-1}): 3647.68, 3461.52, 3303.74, 3168.27, 3051.74, 1620.31, 1535.84, 1578.11, 1468.82, 1434.36, 1319.48, 1245.67, 1188.44, 1159.40, 1095.95, 1026.21, 999.22, 942.26, 726.79, 697.68. Molar conductance (μS cm^{-1}, DMSO): 60.1. Analytical HPLC: acetonitrile (solvent A) and milliQ water (solvent B). T_R = 10.644 min.

[Ru(mbi)(dppm)$_2$]Cl (**4**): 95 mg, 0.09 mmol, 56%. ^{1}H NMR (400 MHz, DMSO-d_6, 298 K) δ/ppm = 8.08–8.00 (m, 2H), 7.89–7.82 (m, 2H), 7.54 (t, *J* = 7.2 Hz, 1H), 7.49–6.98 (m, 25H), 6.88 (dd, *J* = 18.2, 8.2 Hz, 6H), 6.81–6.71 (m, 2H), 6.70–6.59 (m, 3H), 6.45–6.37 (m, 2H), 6.19 (t, *J* = 7.2 Hz, 1H), 5.39–5.27 (m, 2H), 4.87 (d, *J* = 8.2 Hz, 1H), 4.73 (dd, *J* = 26.3, 11.5 Hz, 1H), 4.22 (dd, *J* = 26.3, 11.5 Hz, 1H). ^{13}C NMR (101 MHz, DMSO-d_6, 298 K) δ/ppm = 139.12, 136.31, 134.72, 131.90, 131.80, 131.74, 131.64, 131.55, 131.11, 131.02, 130.57, 130.25, 130.16, 129.91, 129.73, 129.63, 129.18, 128.77, 128.68, 128.30, 128.23, 128.03, 127.93, 127.79, 127.70, 117.27, 117.12, 111.49, 111.44, 44.91, 44.65, 44.45, 44.28, 42.64, 42.56, 42.37, 42.32, 42.17, 42.09. ^{31}P NMR (162 MHz, DMSO-d_6, 298 K) δ/ppm = 1.38–0.40 (m), −3.91–−4.82 (m), −11.75–−14.66 (m), −26.74 (ddd, *J* = 84.4, 44.8, 30.7 Hz). HRMS (ESI) m/z: [M]+ Calcd for $C_{57}H_{49}N_2P_4RuS$ 1019.1605; Found: 1019.1627. Elemental analysis Calcd for $C_{57}H_{49}ClN_2P_4RuS + 0.5H_2O$ (%): C, 62.24; H, 4.67; N, 2.55; Found: C, 62.07; H, 4.66; N, 2.52. UV-Vis (DMSO): λ_{max} (ε×10^3 M^{-1} cm^{-1}): 314 nm (14.6), 356 nm (2.96), 400 nm (1.23). IR: ν(cm^{-1}): 3646.33, 3050.31, 1958.76, 1888.50, 1811.32, 1650.90, 1595.76, 1571.62, 1483.37, 1465.00, 1434.29, 1357.62, 1375.21, 1287.97, 1259.35, 1189.25, 1159.03, 1095.03, 1026.53, 1010.51, 975.75, 999.36, 907.43, 815.83, 843.28, 730.26, 696.33, 616.71. Molar conductance (μS cm^{-1}, DMSO): 61.6. Analytical HPLC: acetonitrile (solvent A) and milliQ water (solvent B). T_R = 13.515 min.

[Ru(mnbi)(dppm)$_2$]Cl (**5**): 80 mg, 0.072 mmol, 45%. ^{1}H NMR (400 MHz, DMSO-d_6, 298 K) δ/ppm = 8.03 (d, *J* = 4.3 Hz, 2H), 7.95 (s, 1H), 7.90–7.75 (m, 2H), 7.63–6.59 (m, 35H), 6.46–6.36 (m, 2H), 5.77 (s, 1H), 5.55–5.43 (m, 1H), 5.43–5.30 (m, 1H), 4.79 (dd, *J* = 26.8, 11.7 Hz, 1H), 4.60 (d, *J* = 8.9 Hz, 1H), 4.31–4.14 (m, 1H). ^{13}C NMR (101 MHz, DMSO-d_6, 298 K) δ/ppm = 151.28, 138.83, 138.50, 137.95, 135.94, 135.53, 134.59, 134.23, 132.48, 132.38, 131.88, 131.78, 131.69, 131.47, 131.39, 131.31, 131.17, 131.09, 131.00, 130.91, 130.55, 130.51, 130.46, 130.00, 129.79, 129.66, 129.56, 129.29, 129.09, 129.01, 128.88, 128.78, 128.64, 128.52, 128.38, 128.29, 128.20, 128.11, 128.01, 127.90, 127.80, 114.37, 113.72, 111.88, 109.31, 108.28, 107.22, 54.97, 44.04, 43.80, 43.62, 43.56, 42.49, 42.24, 42.02, 41.78. ^{31}P NMR (162 MHz, DMSO-d_6, 298 K) δ/ppm = 0.94 (ddd, *J* = 49.9, 44.9, 26.9 Hz), −4.22–−5.00 (m), −11.67–−14.59 (m), −25.61–−28.84 (m). HRMS (ESI) m/z: [M]+ Calcd for $C_{57}H_{48}N_3O_2P_4RuS$ 1064.1456; Found 1064.1471. Elemental analysis Calcd for $C_{57}H_{48}ClN_3O_2P_4RuS$ (%): C, 62.27; H, 4.40; N, 3.82; Found: C, 62.09; H, 4.52; N, 3.96. UV-Vis (DMSO): λ_{max} (ε×10^3 M^{-1} cm^{-1}): 300 nm (17.0), 356 nm (11.6). IR: ν(cm^{-1}): 3667.19, 3054.64, 2918.11, 2661.41, 1972.70, 1898.01, 1811.39, 1753.24, 1652.55, 1572.84, 1588.22, 1458.52, 1484.21, 1434.51, 1310.76, 1362.02, 1285.28, 1248.56, 1158.47, 1189.02, 1124.43, 1096.26, 1025.90, 1058.39, 999.44, 939.73, 846.86, 877.24, 815.17, 728.28, 694.38, 617.03. Molar conductance (μS cm^{-1}, DMSO): 37.6. Analytical HPLC: acetonitrile (solvent A) and milliQ water (solvent B). T_R = 13.261 min.

[Ru(mabi)(dppm)$_2$]Cl (**6**): 80 mg, 0.074 mmol, 46%. ^{1}H NMR (400 MHz, DMSO-d_6, 298 K) δ/ppm = 11.95 (s, 1H), 7.97–7.89 (m, 2H), 7.87–7.76 (m, 2H), 7.60 (t, *J* = 6.9 Hz, 1H), 7.57–6.95 (m, 29H), 6.90 (t, *J* = 7.3 Hz, 2H), 6.82–6.76 (m, 2H), 6.67–6.60 (m, 2H), 6.51–6.36 (m, 2H), 6.31 (dd, *J* = 8.4, 1.9 Hz, 3H), 5.82 (dd, *J* = 8.7, 2.1 Hz, 1H), 5.45 (ddd, *J* = 31.6, 15.7, 7.8 Hz, 2H), 4.92–4.71 (m, 2H), 4.60 (d, *J* = 8.7 Hz, 1H), 4.40–4.23 (m, 1H). ^{31}C NMR (101 MHz, DMSO-d_6, 298 K) δ/ppm = 160.58, 143.92, 138.49, 136.02, 135.61, 134.04, 132.26, 132.18, 132.08, 132.04, 131.86, 131.78, 131.43, 131.18, 130.80, 130.73, 130.63, 130.56, 130.33, 130.22, 130.11, 129.91, 129.61, 129.54, 129.48, 129.39, 129.23, 129.14, 128.95, 128.85, 128.80, 128.70, 128.60, 128.46, 128.36, 124.08, 113.94, 110.22, 110.00, 109.74, 95.30, 94.82, 93.30, 85.14, 82.45, 46.70, 46.48, 45.11, 44.67, 42.83, 42.61, 36.95, 36.77. ^{31}P NMR (162 MHz, DMSO-d_6, 298 K) δ/ppm = 1.28–0.29 (m), −3.17–−4.19 (m), −12.02 (ddd, *J* = 325.8, 46.7, 24.7 Hz), −24.48–−27.42 (m). HRMS (ESI) m/z: [M]+ Calcd for $C_{57}H_{50}N_3P_4RuS$ 1034.1714; Found 1034.1733. Elemental analysis Calcd for $C_{57}H_{50}ClN_3P_4RuS + 0.5CH_3OH$ (%): C, 63.62; H, 4.83; N, 4.21; Found: C, 63.94; H, 5.23; N, 4.21. UV-Vis (DMSO): λ_{max} (ε×10^3 M^{-1} cm^{-1}): 334 nm (17.1) IR: ν(cm^{-1}): 3641.03, 3051.49, 1963.26, 1896.07, 1816.46, 1629.28, 1585.71, 1571.65, 1482.96, 1434.22, 1358.58, 1308.83, 1277.74, 1220.94, 1160.40, 1096.31, 1025.82, 982.59, 999.31, 919.54, 843.81, 727.94, 696.98, 617.09. Molar conductance (μS cm^{-1}, DMSO): 61.8. Analytical HPLC: acetonitrile (solvent A) and milliQ water (solvent B). T_R = 10.865 min.

Partition coefficient. Octanol/PBS partition coefficients (log Po/w) were determined using the shake-flask method. A total of 1 mg of each complex was solubilized in 1000 μL of DMSO and an aliquote of 50 μL was added to a mixture of equal volume of PBS (975 μL) and n-octanol (975 μL). The solutions were continuously shaken for 24 h at 1000 rpm and at 37 °C. Then, the samples were centrifuged for 5 min at 1000 rpm, and the organic and aqueous phases were

separated. The organic phase was measured spectrophotometrically and the concentration was determined from a calibration curve (a linear regression) in order to obtain log P values = [complex(n-octanol)]/[complex(PBS)]. The experiments were carried out in triplicate.

DLS Analysis. The size distributions by intensity and the PDIs were determined by dynamic light scattering (DLS) using a Malvern ZetaSizer Nano ZS (scattering angle = 173°) at a temperature of 25 °C with an equilibrium time of 120 s. Stock solutions (2 mM) of the complexes in DMSO were diluted at a concentration of 20 μM in 10% FBS in PBS.

Cell Culture. Mouse colon adenocarcinoma (CT-26, RRID: CVCL_7254, ATCC: CRL-2638), human colon cancer (HT-29, RRID: CVCL_HT29, ATCC: HTB-38), human lung carcinoma (A-549, RRID: CVCL_A549, ATCC: CCL-185) and non-cancerous retinal pigment epithelium (RPE-1, RRID: CVCL_4388, ATCC: CRL-4000) were used. CT-26 cells were cultured in DMEM, A549 cells were cultured in F-12 K medium, HT-29 cells were cultured in McCoy medium and RPE-1 cells were cultured in DMEM/F-12 medium. All cell lines were supplemented with 10% of fetal bovine serum (FBS), complemented with 100 U/mL penicillin–streptomycin (PS) mixture and maintained in a humidified atmosphere at 37 °C and 5% of CO_2. All cell lines were kindly provided by Dr. Michèle Salmain, Institut parisien de chimie moléculaire, Sorbonne Université, Paris, France. Culture media, FBS and PS mixture obtained from Gibco (Gibco, Life Technologies, USA),

Cytotoxicity. Mouse colon adenocarcinoma (CT-26), human colon cancer (HT-29), human lung carcinoma (A-549) and non-cancerous retinal pigment epithelium (RPE-1) cells were seeded in 96-well plates (100 μL/well). After 24 h, the medium was replaced by test compound dilutions in fresh medium (100 μL/well) and cells were incubated at 37 °C, 5% CO_2. After 48 h of incubation, the medium was removed, and 100 μL of complete medium containing resazurin (0.2 mg/mL final concentration) was added. After 4 h of incubation at 37 °C, the fluorescence signal of the resorufin product was read in a SpectraMax M2 Microplate Reader (λex: 540 nm and λem: 590 nm). Fluorescence data were normalized, data were fitted using GraphPad Prism Software and IC_{50} was calculated by non-linear regression and reported with a standard deviation ($IC_{50} \pm SD$).

Clonogenic survival assay. For the clonogenic assay, A549 lung cancer cells were used. A total of 500 cells were cultured per well in a 6-well plate. After 24 h, compounds **1** and **2** were added in different concentrations. The plates were incubated at 37 °C in 5% CO_2 for 48 h. Then, the culture medium was replaced with a fresh medium and the plates were incubated for an additional 7 days. After this period, the culture medium was removed, and the colonies formed were fixed with a methanol/acetic acid solution of the violet crystal 0.5% for 30 min. Further, the plates were washed with water and dried at room temperature. The test was performed in triplicate. Relative survival was calculated using ImageJ software in the "Colony Area" Plug-in and the "Watershed" and "Analyze Particles" functions. The parameters size (0.01-infinity) and circularity (0.30–1.00) were employed.

Cell migration assay. To evaluate the A549 cell migration inhibition ability, we used the wound healing assay, where 2.0×10^5 cells per well were seeded in a 6-well plate maintained at 37 °C in a 5% CO_2 atmosphere for 24 h. After incubation, a wound was made using a sterile 1 mL pipette. The culture medium was changed, and compounds **1** and **2** were added at $\frac{1}{2}$ IC_{50} concentration (μM). The images were taken at times of 0, 24 and 48 h using an inverted optical microscope (NIKON ECLIPSE TS100) with a 4× objective lens, coupled with a Motcam 1SP camera.

Cellular uptake. A549 cells were seeded at a density of 1×10^6 cells per well. The next day, cells were treated with 1 and 10 μM of the corresponding Ru compound diluted in the cell culture medium from a 10 mM stock solution in DMSO. After 45 min and 4 h, cells were collected, counted, and stored at −80 °C. These samples were digested using 70% nitric acid (500 μL, 65 °C, overnight), and 100 μL of this mix were dissolved in 3 mL of pure water and analyzed using ICP-MS.

DNA metallation. A549 cells were seeded at a density of 7.5×10^5 cells per well. The next day, cells were treated with 10 μM of the corresponding Ru compound diluted in the cell culture medium from a 10 mM stock solution in DMSO. After 4 h, cells were collected, counted, and stored at −80 °C. These samples were digested using 70% nitric acid (500 μL, 65 °C, overnight), and 100 μL of this mix were dissolved in 3 mL of pure water and analyzed using ICP-MS.

ICP-MS Studies. All ICP-MS measurements were performed on an Agilent 7900 Quadrupole ICP-MS located at the Institut de Physique du Globe de Paris, France. The monitored isotopes are 99 and 101 Ru. Daily, before the analytical sequence, an indium internal-standard was injected after inline mixing with the samples to correct for signal drift and matrix effects. A set of calibration standards was analyzed to confirm and model (through simple linear regression) the linear relationship between signal and concentration. The model was then used to convert measured sample counts to concentrations. Reported uncertainties were calculated using error propagation equations and considering the combination of standard deviation on replicated consecutive signal acquisitions (n = 3), internal-standard ratio and blank subtraction. The non-linear term (internal-standard ratio) was linearized using a first-order Taylor series expansion to simplify error propagation. The amount of metal detected in the cell samples was transformed from ppb to μg of metal. Data were subsequently normalized to the number of cells and expressed as ng or % of metal per million cells.

JC-1 Mitochondria Membrane Potential Test. A549 cells were seeded at a density of 1×10^4 cells/well in black 96-well plates (Corning) and maintained at 37 °C in a 5% CO_2 atmosphere for 24 h. After incubation, cells were treated with different concentrations of **1** and **2** ($\frac{1}{2}$ IC_{50} and IC_{50} concentrations). After another 24 h, the medium was removed and treated with a JC-1 solution (100 μL, culture medium without phenol red) and maintained at 37 °C in a 5% CO_2 atmosphere for 30 min. After incubation, the cells were washed with PBS, the fluorescence signal of JC-1 was read using a Synergy/H1-Biotek fluorometer (aggregate, Ex/Em: 535/590 nm and monomer, Ex/Em: 475/530 nm), and the images were taken using a CELENA® S Digital Imaging System (Logos Biosystems). The data were analyzed using GraphPad Prism software 8.0.2.

Mito stress test. A549 cells were seeded in Seahorse XFe 96-well plates at a density of 20 000 cells/well in 80 μL of the medium. After 24 h, the medium was replaced with fresh medium, and the corresponding complex (**1** or **2**) was added. After 4 h of incubation, the regular medium was removed, and cells were washed three times using Seahorse base medium containing pyruvate 1 mM, glutamine 2 mM and glucose 10 mM, and incubated in a non-CO_2 incubator at 37 °C for 1 h. A Mito stress assay was run after adding 1 μM oligomycin, 1 μM FCCP, and a mixture of 1 μM antimycin-A/1 μM rotenone in ports A, B and C, respectively, using a Seahorse XFe96 extracellular flux analyzer.

Statistical Analysis. IC_{50} values are expressed as mean ± SD (n = 3). ICP-MS results are presented as mean ± SD of two independent replicates. Biological experiments are expressed with n = 3 (for

clonogenic assay) or n = 6 (for JC-1 assay), with a one way ANOVA test followed by Dunnett's test. Data are expressed as means ± SD (** $P < 0.01$ and **** $P < 0.0001$).

Acknowledgements

We thank the São Paulo State Research Support Foundation (FAPESP, Grants 2023/02475-8 and 2022/02876-0) and CNPq for financial support. M. V. P.-M. thanks FAPESP (Grants 2021/01787-0 and 2022/09971-8). This work was financially supported by an ERC Consolidator Grant PhotoMedMet to G. G. (GA 681679) and has received support under the program "Investissements d'Avenir" launched by the French Government and implemented by the ANR with the reference ANR-10-IDEX-0001-02 PSL (G. G.). The quadrupole ICP-MS belongs to the PARI platform and its access and use is regulated by the PARI charter. Parts of this work were supported by IPGP multidisciplinary program PARI, and by Paris–IdF region SESAME Grant no. 12015908.

Conflict of Interests

The authors declare no conflict of interest.

Data Availability Statement

The data that support the findings of this study are available in the supplementary material of this article.

Keywords: bioinorganic chemistry · cancer · medicinal inorganic chemistry · metals in medicine · mitochondrial respiration · ruthenium(II)

[1] B. A. Chabner, T. G. Roberts Jr, *Nat. Rev. Cancer* **2005**, *5*, 65–72. DOI: 10.1038/nrc1529.
[2] L. Kelland, *Nat. Rev. Cancer* **2007**, *7*, 573–584. DOI: 10.1038/nrc2167.
[3] R. Oun, Y. E. Moussa, N. J. Wheate, *Dalton Trans.* **2018**, *47*, 6645–6653. DOI: 10.1039/C8DT00838H.
[4] E. Boros, P. J. Dyson, G. Gasser, *Chem.* **2020**, *6*, 41–60. DOI: 10.1016/j.chempr.2019.10.013.
[5] K. J. Franz, N. Metzler-Nolte, *Chem. Rev.* **2019**, *119*, 727–729. DOI: 10.1021/acs.chemrev.8b00685.
[6] E. J. Anthony, E. M. Bolitho, H. E. Bridgewater, O. W. L. Carter, J. M. Donnelly, C. Imberti, E. C. Lant, F. Lermyte, R. J. Needham, M. Palau, P. J. Sadler, H. Shi, F.-X. Wang, W.-Y. Zhang, Z. Zhang, *Chem. Sci.* **2020**, *11*, 12888. DOI: 10.1039/D0SC04082G.
[7] S. Y. Lee, C. Y. Kim, T.-G. Nam, *Drug Des. Dev. Ther.* **2020**, *14*, 5375–5392. DOI: 10.2147/DDDT.S275007.
[8] Pragti, B. K. Kundu, S. Mukhopadhyay, *Coord. Chem. Rev.* **2021**, *448*, 214169. DOI: 10.1016/j.ccr.2021.214169.
[9] M. Martínez-Alonso, G. Gasser, *Coord. Chem. Rev.* **2021**, *434*, 213736. DOI: 10.1016/j.ccr.2020.213736.
[10] A. Notaro, G. Gasser, *Chem. Soc. Rev.* **2017**, *46*, 7317. DOI: 10.1039/c7cs00356k.
[11] M. M. Da Silva, G. H. Ribeiro, M. S. De Camargo, A. G. Ferreira, L. Ribeiro, M. I. F. Barbosa, V. M. Deflon, S. Castelli, A. Desideri, R. S. Corrêa, A. B. Ribeiro, H. D. Nicolella, S. D. Ozelin, D. C. Tavares, A. A. Batista, *Inorg. Chem.* **2021**, *60*, 14174–14189. DOI: 10.1021/acs.inorgchem.1c01539.
[12] R. J. Mitchell, A. S. Gowda, A. G. Olivelli, A. J. Huckaba, S. Parkin, J. M. Unrine, V. Oza, J. S. Blackburn, F. Ladipo, D. K. Heidary, E. C. Glazer, *Inorg. Chem.* **2023**, *62*(28), 10940–10954. DOI: 10.1021/acs.inorgchem.3c00736.
[13] G. H. Ribeiro, A. P. M. Guedes, T. D. De Oliveira, C. R. S. T. B. De Correia, L. Colina-Vegas, M. A. Lima, J. A. Nóbrega, M. R. Cominetti, F. V. Rocha, A. G. Ferreira, E. E. Castellano, F. R. Teixeira, A. A. Batista, *Inorg. Chem.* **2020**, *59*, 15004–15018. DOI: 10.1021/acs.inorgchem.0c01835.
[14] N. P. Da Silva, M. V. Palmeira-Mello, N. Oliveira Acésio, C. A. F. Moraes, J. Honorato, E. Castellano, D. C. Tavares, K. M. M. De Oliveira, A. A. Batista, *Dalton Trans.* **2025**, DOI: 10.1039/D4DT02575J.
[15] D. C. Wallace, *Nat. Rev. Cancer* **2012**, *12*(10), 685–698. DOI: 10.1038/nrc3365.
[16] J. S. Modica-Napolitano, V. Weissig, *Int. J. Mol. Sci.* **2015**, *16*, 17394–17421. DOI: 10.3390/ijms160817394.
[17] P. E. Porporato, N. Filigheddu, J. M. Bravo-San Pedro, G. Kroemer, L. Galluzzi, *Cell Res.* **2018**, *28*, 265–280. DOI: 10.1038/cr.2017.155.
[18] J. Cervinka, A. Gobbo, L. Biancalana, L. Markova, V. Novohradsky, M. Guelfi, S. Zacchini, J. Kasparkova, V. Brabec, F. Marchetti, *J. Med. Chem.* **2022**, *65*(15), 10567–10587. DOI: 10.1021/acs.jmedchem.2c00722.
[19] G. F. Grawe, K. M. Oliveira, C. M. Leite, T. D. De Oliveira, J. Honorato, A. G. Ferreira, E. Castellano, M. R. Cominetti, R. S. Correa, A. A. Batista, *Dalton Trans.* **2022**, *51*, 1489–1501. DOI: 10.1039/D1DT02851K.
[20] K. M. Oliveira, E. J. Peterson, M. C. Carroccia, M. R. Cominetti, V. M. Deflon, N. P. Farrell, A. A. Batista, R. S. Correa, *Dalton Trans.* **2020**, *49*, 16193. DOI: 10.1039/d0dt01091j.
[21] K. M. Oliveira, J. Honorato, G. R. Gonçalves, M. R. Cominetti, A. A. Batista, R. S. Correa, *Dalton Trans.* **2020**, *49*(36), 1264312652. DOI: 10.1039/D0DT01591A.
[22] B. N. Cunha, L. Colina-Vegas, A. M. Plutín, R. G. Silveira, J. Honorato, K. M. Oliveira, M. R. Cominetti, A. G. Ferreira, E. E. Castellano, A. A. Batista, *J. Inorg. Biochem.* **2018**, *186*, 147–156. DOI: 10.1016/j.jinorgbio.2018.06.007.
[23] V. D. S. Velozo-Sá, L. R. Pereira, A. P. D. Lima, F. Mello-Andrade, M. D. R. M. Rezende, R. M. Goveia, W. C. Pires, M. M. Silva, K. Oliveira, A. G. Ferreira, J. A. Ellena, V. M. Deflon, C. Grisolia, A. A. Batista, E. D. P. Silveira-Lacerda, *Dalton Trans.* **2019**, *48*, 6026–6039, DOI: 10.1039/C8DT03738H.
[24] M. T. Bautista, E. P. Cappellani, S. D. Drouin, R. H. Morreis, C. T. Schweitzer, A. Sella, J. Zubkowski, *J. Am. Chem. Soc.* **1991**, *113*, 4876–4887. DOI: 10.1021/ja00013a025.
[25] W. J. Geary, *Coord. Chem. Rev.* **1971**, *7*, 81–122.
[26] R. Vinck, A. Gandioso, P. Burckel, B. Saubamea, K. Cariou, G. Gasser, *Inorg. Chem.* **2022**, *61*, 13576–13585. DOI: 10.1021/acs.inorgchem.2c02214.
[27] A. Notaro, G. Gasser, A. Castonguay, *ChemMedChem* **2020**, *15*, 345–348, DOI: 10.1002/cmdc.201900677.
[28] M. V. Palmeira-Mello, A. R. Costa, L. P. De Oliveira, O. Blacque, G. Gasser, A. A. Batista, *Dalton Trans.* **2024**, *53*, 10947–10960. DOI: 10.1039/D4DT01191K.
[29] H. Rafehi, C. Orlowski, G. T. Georgiadis, K. Ververis, A. El-Osta, T. C. Karagiannis, *J. Visualization* **2011**, *49*, e2573. DOI: 10.3791/2573.
[30] M. R. S. De Melo, A. B. Ribeiro, G. Fernandes, I. S. Squarisi, M. M. Junqueira, A. A. Batista, M. M. Da Silva, D. C. Tavares, *J. Biol. Inorg. Chem.* **2024**, *29*, 159–168. DOI: 10.1007/s00775-023-02036-8.
[31] C. A. Puckett, J. K. Barton, *J. Am. Chem. Soc.* **2007**, *129*(1), 46–47. DOI: 10.1021/ja0677564.
[32] A. Notaro, M. Jakubaszek, N. Rotthowe, F. Maschietto, R. Vinck, P. S. Felder, B. Goud, M. Tharaud, I. Ciofini, F. Bedioui, R. F. Winter, G. Gasser, *J. Am. Chem. Soc.* **2020**, *142*, 6066–6084. DOI: 10.1021/jacs.9b12464.
[33] M. Han, M. R. Vakili, H. S. Abyaneh, O. Molavi, R. Lai, A. Lavasanifar, *Mol. Pharmaceutics* **2014**, *11*, 2640–2649. DOI: 10.1021/mp500038g.
[34] L. Chen, G. Li, F. Peng, X. Jie, G. Dongye, K. Cai, R. Feng, B. Li, Q. Zeng, K. Lun, J. Chen, B. Xu, *Oncotarget* **2016**, *7*(49), 80716–80734, DOI: 10.18632/oncotarget.13032.
[35] V. R. Silva, R. S. Corrêa, L. S. Santos, M. B. P. Soares, A. A. Batista, D. P. Bezerra, *Sci. Rep.* **2018**, *8*, 288. DOI: 10.1038/s41598-017-18639-6.
[36] J. Zhang, E. Nuebel, D. R. R. Wisidagama, K. Setoguchi, J. S. Hong, C. M. Van Horn, S. S. Imam, L. Vergnes, C. S. Malone, C. M. Koehler, M. A. Teitell, *Nat. Protoc.* **2012**, *7*, 1068–1085. DOI: 10.1038/nprot.2012.048.
[37] J. Karges, F. Heinemann, M. Jakubaszek, F. Maschietto, C. Subecz, M. Dotou, R. Vinck, O. Blacque, M. Tharaud, B. Goud, E. V. Zahínos, B. Spingler, I. Ciofini, G. Gasser, *J. Am. Chem. Soc.* **2020**, *142*, 6578–6587. DOI: 10.1021/jacs.9b13620.

[38] Y. Abe, T. Sakairi, H. Kajiyama, S. Shrivastav, C. Beeson, J. B. Kopp, *Am. J. Physiol. Cell Physiol.* **2010**, *299*, C464–C476. DOI: 10.1152/ajpcell.00563.2009.
[39] J. H. Kim, S. Ofori, S. Parkin, H. Vekaria, P. G. Sullivan, S. G. Awuah, *Chem. Sci.* **2021**, *12*, 7467. DOI: 10.1039/d1sc01418h.
[40] Z. Zhu, Z. Wang, C. Zhang, Y. Wang, H. Zhang, Z. Gan, Z. Guo, X. Wang, *Chem. Sci.* **2019**, *10*, 3089. DOI: 10.1039/c8sc04871a.
[41] M. D. Brand, D. G. Nicholls, *Biochem. J.* **2011**, *435*, 297–312. DOI: 10.1042/BJ20110162.
[42] R. C. Clark, J. S. Reid, *Acta Crystallogr. Sect. A* **1995**, *51*, 887. DOI: 10.1107/S0108767395007367.
[43] CrysAlisPro (version 1.171.42.75a), Rigaku Oxford Diffraction Ltd, Yarnton, Oxfordshire, England, **2022**.
[44] O. V. Dolomanov, L. J. Bourhis, R. J. Gildea, J. A. K. Howard, H. Puschmann, *J. Appl. Crystallogr.* **2009**, *42*, 339. DOI: 10.1107/S0021889808042726.
[45] G. M. Sheldrick, *Acta Crystallogr. Sect. A* **2015**, *71*, 3–8. DOI: 10.1107/S2053273314026370.
[46] G. M. Sheldrick, *Acta Crystallogr. Sect. C* **2015**, *71*, 3–8. DOI: 10.1107/S2053229614024218.
[47] A. L. Spek, *Acta Crystallogr. Sect. D* **2009**, *65*, 148. DOI: 10.1107/S090744490804362X.

Manuscript received: September 7, 2024
Revised manuscript received: December 23, 2024
Accepted manuscript online: January 2, 2025
Version of record online: ■■, ■■

RESEARCH ARTICLE

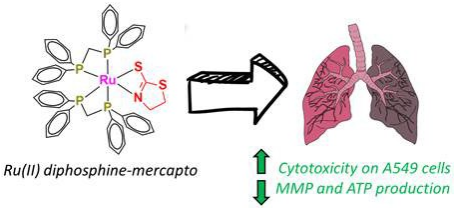

M. V. Palmeira-Mello, P. Mesdom, P. Burckel, S. Hidalgo, O. Blacque, G. Gasser*, A. A. Batista**

Ruthenium(II)-based compounds containing diphosphines and mercapto ligands are cytotoxic and are able to inhibit the colony formation and the migration on A549 lung cancer cells. JC-1 and Mito stress tests revealed these compounds affect the mitochondrial membrane potential, changing the oxygen consumption and ATP levels, confirming mitochondrial dysfunction on these cells.